

# Intein-assisted bisection mapping systematically splits proteins for Boolean logic and inducibility engineering

Trevor Y. H. Ho<sup>1,2</sup>, Alexander Shao<sup>1,2,5</sup>, Zeyu Lu<sup>1,2</sup>, Harri Savilahti<sup>3</sup>, Filippo Menolascina<sup>2,4</sup>, Lei Wang<sup>6</sup>, Neil Dalchau<sup>5</sup> & Baojun Wang<sup>1,2\*</sup>

<sup>1</sup>School of Biological Sciences, University of Edinburgh, Edinburgh, EH9 3FF, UK

<sup>2</sup>Centre for Synthetic and Systems Biology, University of Edinburgh, Edinburgh, EH9 3FF, UK

<sup>3</sup>Department of Biology, University of Turku, Turku, Finland

<sup>4</sup>Institute for Bioengineering, School of Engineering, University of Edinburgh, Edinburgh, EH9 3BF, UK

<sup>5</sup>Microsoft Research, Cambridge, CB1 2FB, UK

<sup>6</sup>School of Engineering, Westlake University, Hangzhou 310024, Zhejiang Province, China

\*To whom correspondence can be addressed. Email: [baojun.wang@ed.ac.uk](mailto:baojun.wang@ed.ac.uk)

## 1 Abstract

2 Split inteins are powerful tools for seamless ligation of synthetic split proteins. Yet, their use remains  
3 limited because the already intricate split site identification problem is often complicated by the  
4 requirement of extein junction sequences. To address this, we augmented a mini-Mu transposon-based  
5 screening approach and devised the intein-assisted bisection mapping (IBM) method. IBM robustly  
6 revealed clusters of split sites on five proteins, converting them into AND or NAND logic gates. We further  
7 showed that the use of inteins expands functional sequence space for splitting a protein. We also  
8 demonstrated the utility of our approach over rational inference of split sites from secondary structure  
9 alignment of homologous proteins. Furthermore, the intein inserted at an identified site could be  
10 engineered by the transposon again to become partially chemically inducible, and to some extent enabled  
11 post-translational tuning on host protein function. Our work offers a generalizable and systematic route  
12 towards creating split protein-intein fusions and conditional inteins for protein activity control.

13 Keywords: split protein, split intein, bisection mapping, logic gates, inducibility, post-translational control

## 14 Introduction

15 Synthetic split proteins are useful tools for biologists<sup>1</sup>. Often, they are created to serve as sensors for  
16 protein-protein interaction<sup>2</sup>, detectors for biomolecules<sup>3, 4</sup>, molecular switches<sup>5, 6</sup>, and logic gates in  
17 synthetic circuits<sup>7-10</sup>. In other instances, proteins are split to be endowed with temporal-spatial<sup>11</sup> or user-  
18 defined controls<sup>12</sup>, or to reduce their sizes for viral delivery<sup>13</sup>. Generation of split proteins invariably  
19 demands the resulting bipartite sections remain individually inactive, and that they can reconstitute  
20 spontaneously or with external assistance, followed by the restoration of protein function<sup>1</sup>.

21 A specific niche of split protein engineering concerns the use of an intein as the driver for split parts  
22 reconstitution. Inteins are internal protein elements that are expressed as part of a larger precursor  
23 protein<sup>14-16</sup>. Upon proper folding, an intein excises itself from the precursor protein and ligates the flanking  
24 external proteins (exteins) with a peptide bond, producing a product as if the intein was absent from the  
25 original gene sequence. An intein split at an appropriate position generates a bipartite intein that can  
26 spontaneously self-assemble and undergo the splicing process. Split inteins thus enable reconstitution of  
27 separate coding sequences with minimal scarring, reducing the chances of additionally inserted residues or

28 domains that might compromise the original functionality upon protein reconstitution. Documented uses  
29 of protein split by inteins include in vivo DNA sensors<sup>17</sup>, protein-based logic gates for bio-computation<sup>18, 19</sup>  
30 and enforcing dual conditions in directed evolution<sup>20</sup>.

31 One of the major challenges in splitting proteins is the identification of split sites that ensure function loss  
32 in split parts but permit protein reconstitution. The use of inteins introduces an extra layer of complexity –  
33 inteins require specific extein junction sequences for efficient splicing<sup>21, 22</sup>. Hence, the composition of amino  
34 acid residues around a chosen split site needs to be carefully considered. Alternatively, one can insert  
35 characterized extein junctions at a putative split site, or modify host protein residues around a putative  
36 split site to satisfy extein junction requirements. Doing so could risk perturbations to the protein structure  
37 and function. By either approach, the split site design space is often sparsely sampled by educated guesses  
38 with split sites tested through trial-and-error<sup>6, 23, 24</sup>, which is inefficient. A better solution would be to  
39 predict split sites computationally from protein crystal structures. A method was recently developed to  
40 predict intein-insertable split sites by searching flexible regions on protein structures and regions that lack  
41 functional conservation<sup>25</sup>. This was demonstrated on antibiotic resistance genes. Another method, SPELL<sup>26</sup>,  
42 takes protein structures, calculates split energies and identifies surface-exposed loops that contains low  
43 conservation in sequences to predict split sites. SPELL was designed to split proteins with a pair of  
44 chemically inducible dimerization (CID) domain, but the principle behind might be general enough for use  
45 with inteins. While these computational methods provided better rationality in testing split sites, they  
46 require 3D structures. If crystal structures are unavailable homology modelling could be used to generate  
47 predicted protein structures, but using predicted structures as inputs might reduce prediction accuracy.

48 To facilitate split site identification without knowing protein structures, we customized and improved  
49 previously described mini-Mu transposon-based approaches<sup>27-31</sup>. We developed a bisection mapping  
50 method that involves the fusion of a pair of split intein to the bisected host protein parts. The technique  
51 was applied to four proteins and revealed novel split sites for achieving the AND and NAND logic. We  
52 highlighted the advantage of using an intein compared to interacting domains in splitting proteins,  
53 employed our method to evaluate a single case of split site prediction from protein structural homology,  
54 and described suppressing uninduced activities by splitting highly active proteins. Finally, we demonstrated  
55 in principle that, once functional split sites for an intein are identified, some degree of post-translational  
56 inducibility can be engineered into the intein to achieve drug-dependent control of protein function.

## 57 **Results**

### 58 **Designing the IBM workflow for split site screening**

59 In pursuit of a systematic protocol to search for split sites for inteins, we built upon existing methods  
60 utilizing the mini-Mu transposon, bisection mapping<sup>27</sup> (BM) and domain-insertion profiling<sup>28, 29</sup> (DIP), and  
61 incorporated features from the latter into the former. In brief, the method (**Fig. 1a, Supplementary Fig. 1**)  
62 starts with an in vitro transposition reaction that randomly inserts a BbsI and SapI-flanked transposon into a  
63 staging vector, which hosts a slightly trimmed, BsaI-flanked coding DNA sequence (CDS) of interest  
64 (**Supplementary Fig. 2**). This is followed by size selection of the insertion library such that only CDS  
65 fragments with insertions would be isolated and ligated into a vector for protein expression. A Golden Gate  
66 reaction is then used to irreversibly substitute the transposon with a DNA fragment. The fragment carries a  
67 selection marker, a split intein, and transcription and translation initiation elements for carboxyl-lobe (C-  
68 lobe) expression. In-frame insertions in the right orientation would thus split a CDS into two with the  
69 amino-lobes (N-lobes) and C-lobes of the split intein as fusion partners, under separate control of two  
70 inducible promoters. The final library is then screened for individual clones that display functional activities  
71 only when the chemical inducers for both promoters are present. The clones are then sequenced at the  
72 fusion joints to reveal the split sites.

73 For the split intein, we selected the *Ssp* DnaB<sup>M86</sup> intein<sup>32</sup> (thereafter referred as the M86 intein) since it only  
74 requires the -1 and +1 extein residues for splicing. These extein residues are incorporated into the  
75 substitution insert. Successful splicing of the M86 intein would leave behind a highly predictable four-  
76 residue peptide linker at the split site of the original protein (**Supplementary Fig. 3**). Our method is an  
77 augmentation of BM by an intein – hence the name intein-assisted bisection mapping (IBM).

## 78 mCherry as a proof of concept for the IBM workflow

79 To preempt potential difficulties in troubleshooting if the IBM workflow returned no functional split sites,  
80 we first carried out a proof of principle test utilizing mCherry as the target protein to be split. mCherry has  
81 been employed as a reporter for Bimolecular Fluorescent Complementation (BiFC) and two split sites,  
82 159/160 and 174/175, were known to create bipartite lobes that would regain functionality if brought into  
83 proximity<sup>33</sup>. We created a split mCherry construct that simulated the known split site 159/160 being  
84 sampled by IBM. This construct only gave increased fluorescence when the inputs for N- (inducible by  
85 arabinose) and C-lobes (inducible by AHL) were present (**Supplementary Fig. 4**). Thus, provided enough  
86 library coverage, a successful execution of the IBM workflow should generate the simulated control as a  
87 member within the final library, and the control should be recoverable afterwards.

88 Given the assurance, we proceeded to run the IBM workflow on the mCherry protein (**Fig. 1a**). The resulting  
89 library was induced with both arabinose and AHL. Cells with fluorescence above autofluorescence were  
90 sorted by fluorescence-activated cell sorting (FACS), plated and isolated as single colonies. Individual strains  
91 were then assayed for responses in the absence or presence of the two inducers, and those that showed  
92 AND logic behavior were subsequently sequenced to identify the split sites. Pooling the results yielded an  
93 intein-bisection map (**Fig. 1b, Supplementary Fig. 5**). A total of 15 split sites were identified. At all sites,  
94 protein splicing was proven by a Western blot (**Supplementary Fig. 6**). All split sites clustered into 4 seams,  
95 which were mostly located on loops between the  $\beta$  sheets of the barrel. The second and the third seams  
96 should cover sites 159/160 and 174/175, though curiously, site 159/160 was not sampled by this IBM  
97 attempt. This site was present in the library we screened (**Supplementary Table 1**) and was left out  
98 fortuitously, likely due to under sampling.

99 To our knowledge, the seams 121/122 and 185/186 – 194/195 were never described to contain functional  
100 split sites before. Of equal interest was the fact that four split sites, while close to the loops, were found  
101 between amino acids that constituted the  $\beta$  sheets (**Fig. 1c**), and this could suggest tolerance of either  
102 structural disruption or inserted linkers, both of which are unlikely to be ever attempted if split sites were  
103 designed rationally. Together, these two observations showcased that IBM has the potential to discover  
104 novel and unexpected split sites.

105 We also noticed that sites within seam 185/186 – 194/195 yielded a low level of fluorescence when the  
106 cells were grown under prolonged induction (24 h) of the N-lobe alone. Other bipartite mCherry split at  
107 other seams did not show such behavior. This might be explained by a leaky  $P_{lux2}$  promoter, and the fact  
108 that mCherry split at the last seam would produce relatively shorter C-lobes that were easier to transcribe  
109 and translate.

110 Since the literature reported split sites on mCherry were developed for bimolecular fluorescent  
111 complementation<sup>33</sup>, we asked whether the new split sites identified could serve the same purpose. We  
112 arbitrarily selected one or two representative split sites from each seam. We also included three additional  
113 sites that were found within  $\beta$ -sheets. For each site, we built split mCherry constructs where the split M86  
114 intein was removed or replaced by a pair of synthetic and heterodimerizing coil-coiled domains, SYNZIP17  
115 and SYNZIP18<sup>34</sup> (**Fig. 1d, Supplementary Fig. 7**). For all constructs where split sites were on flexible loops,  
116 increase in fluorescence could be observed when both lobes were expressed with SYNZIPs, demonstrating  
117 that for mCherry, tolerances of the IBM-identified split sites to protein fusion were not unique to the intein.  
118 Sites within  $\beta$ -sheets, except 176/177, did not yield an increase in fluorescence, likely due to structural

119 disruptions to the  $\beta$ -barrel. To test whether the N- and C-lobes could complement without external help  
120 from SYNZIPs, we removed SYNZIP17 from the N-lobes and conducted the experiment. Results showed no  
121 increase in fluorescence and Western blots proved that it was not due to lack of protein expression.

#### 122 **IBM identified a computationally unpredicted split site on $\beta$ -lactamase**

123 Since a computational method<sup>25</sup> exists to predict split sites for the gp41-1 intein<sup>35</sup> on antibiotic resistance  
124 genes, we asked how a library approach through IBM would perform in comparison to a computational  
125 approach. We focused on the case of TEM-1  $\beta$ -lactamase (also abbreviated as BLA in figures). It has a  
126 resolved crystal structure and a well-established split site at 194/196<sup>36</sup> or 195/196<sup>37</sup>. The previously  
127 mentioned computational method identified a new split site at 104/105, which when used with the split  
128 gp41-1 intein, allowed co-selection of two plasmids with just ampicillin<sup>25</sup>. We therefore sought to recover  
129 these two sites with IBM. We employed the gp41-1 intein with the -2, -1 and +1, +2 minimal extein residues  
130 (GY/SS)<sup>38</sup> and passed  $\beta$ -lactamase through the IBM pipeline. Split clones that conferred ampicillin resistance  
131 were enriched through selection and outgrowth. Subsequent sequencing on candidate clones revealed 6  
132 split sites on 2 split seams (**Supplementary Fig. 8**). The first seam, consisting sites 192/193 and 196/197  
133 corresponded to the established site of 195/196. Whereas the second seam (260/261, 261/262, 264/265,  
134 267/268) represented a previously unreported split location. We noted that the absence of the  
135 computationally predicted site 104/105 could be due to the clones being outcompeted during the  
136 enrichment process. Hence, IBM was not necessarily superior to computational methods, but could  
137 complement them in identifying more intein-insertable split sites.

138

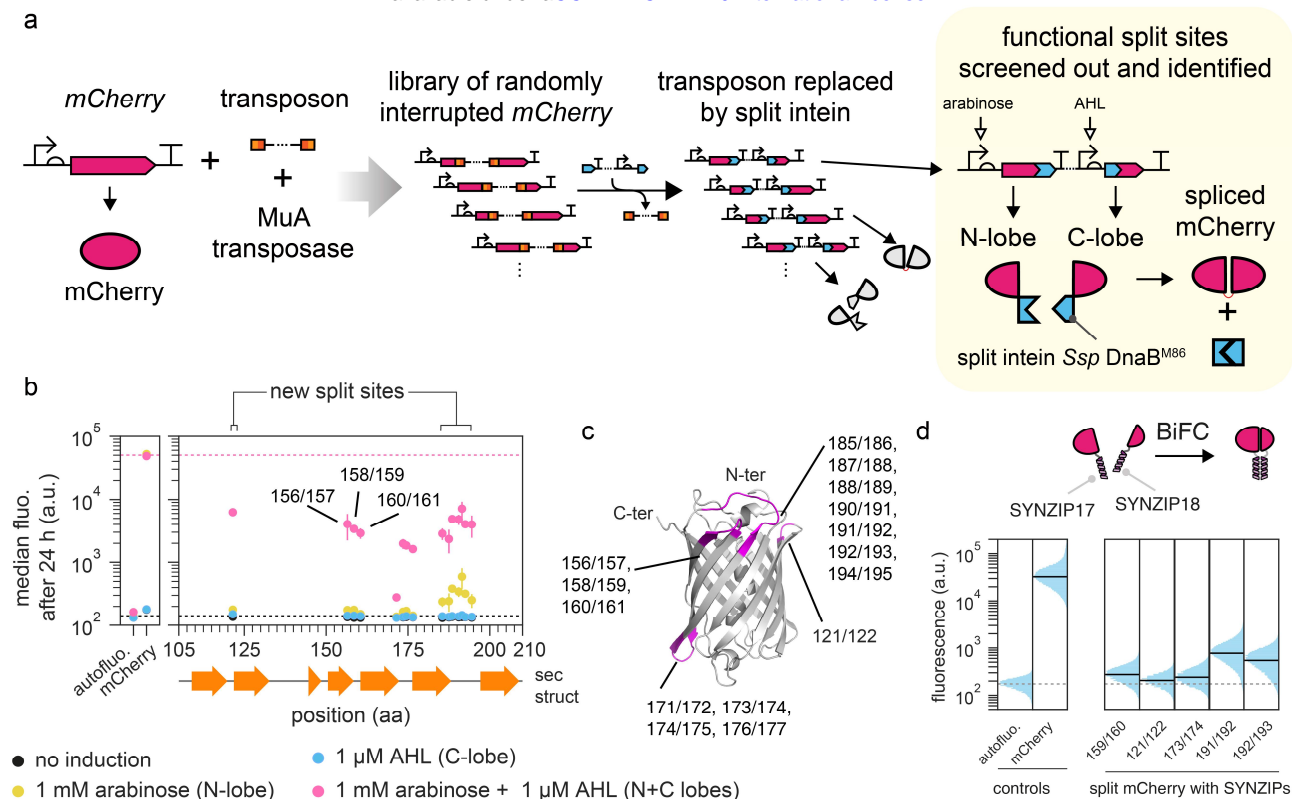


**Fig. 1 Proof-of-concept of InteIn-assisted Bisection Mapping (IBM) on mCherry to recover known split sites for BiFC and discover new ones.** **a.** Workflow. A transposon was randomly inserted into the mCherry CDS, and was then substituted with a DNA fragment containing the split intein *Ssp DnaB<sup>M86</sup>*. This generated a library of mCherry-split intein fusions that can be screened for fluorescence only when both the N and C-lobes were expressed. **b.** Two new loops for split sites were identified within mCherry and two existing ones were recovered. Each vertical group of spots represents an identified split site, aligned to the mCherry secondary structure below. The majority of sites are between the  $\beta$ -sheets of the barrel.  $\bar{y}$  locations and error bars are mean and std of median fluorescence from experiments performed on 3 different days. Horizontal dashed lines bound the range of fluorescence that split mCherry could yield. See **Supplementary Fig. 5** for site distributions and activities at 5 h. **c.** Split sites mapped to a reconstructed mCherry 3D structure (PDB: 2H5Q). Each split site has the -1 and the +1 amino acid residues colored. **d.** Representative split sites from each loop on mCherry permitted biomolecular fluorescence complementation (BiFC). Single-cell fluorescence values were pooled from 3 biological replicates. Solid black horizontal lines denote population median, except for autofluorescence which was denoted by dotted grey lines.

### 139 **Applying IBM to engineer AND and NAND logic gates**

140 Having established the IBM workflow, we then sought to demonstrate its universality in engineering  
141 protein-based logic gates<sup>10, 39, 40</sup>. We focused on transcription factors because their responses could be  
142 directly converted to an assayable fluorescent output (**Fig. 2a**). We chose the repressor TetR and its  
143 homolog SrpR from the same protein family<sup>41</sup>, and an activator, the extra cytoplasmic sigma factor 20  
144 (ECF20)<sup>42</sup>. Each protein was fed into the IBM workflow using the M86 intein and a corresponding intein-  
145 bisection map was generated. 3 split seams and 32 split sites were found for TetR; 4 seams and 13 sites for  
146 SrpR; 3 seams and 17 sites for ECF20 (**Fig. 2b-d, Supplementary Fig. 10-12**). Most of the split sites for TetR  
147 clustered around loop regions between helices from the TetR crystal structure (PDB: 4AC0, **Supplementary**  
148 **Fig. 13**). It is noteworthy that the same was observed for SrpR and ECF20 even though their shown  
149 secondary structures were only predictions that we generated from JPred4<sup>43</sup>. The performance of the logic  
150 gates in aspect of on and off states strongly depends on the split protein, the split site locations as well as  
151 the time elapsed since induction. Across most split sites found in TetR and ECF20, the split proteins would  
152 show qualitative NAND and AND gate behavior with good repression and activation strengths at both 5 and  
153 24 h. For SrpR, most split sites yielded NAND gate behavior at 5 h post-induction with observable levels of  
154 repression, but at 24 h, expression of C-lobes alone sufficed to evoke a strong repression rendering the  
155 circuit more like a single input responsive gate (**Supplementary Fig. 11**). This was caused by an  
156 accumulation of the N-lobes from leaky  $P_{araBAD}$  expression over time and the NAND behavior could be  
157 restored by eliminating the leakiness (**Supplementary Fig. 13**), proving that either N- or C-lobe alone was  
158 capable of repression. Our results thus demonstrated that the IBM workflow is generally applicable and  
159 could return multiple sites for choosing the most appropriate gates for user-defined applications.

### 160 **IBM indirectly defined functional boundaries on the ECF20 activator protein**

161 While screening the colonies for AND gates in ECF20, we observed that 80% yielded strong activation  
162 activities from the expression of N-lobes alone (data not shown), which emulated the responses of an intact  
163 protein and addition of C-lobes did not further improve activities. We thus surmised that they could be  
164 truncations at the C-termini and sequenced some of them. Indeed, those split sites were clustered at 178-  
165 185 (**Fig. 2d**) and approximately corresponded to the end of the last helix on ECF20, suggesting that the  
166 residues beyond position 178 could be trimmed without loss of function. In contrast, the first helix was  
167 crucial since the first AND gate split site was found immediately after it. These two observations suggested  
168 that IBM could be repurposed to determine the minimal functional size of a protein.

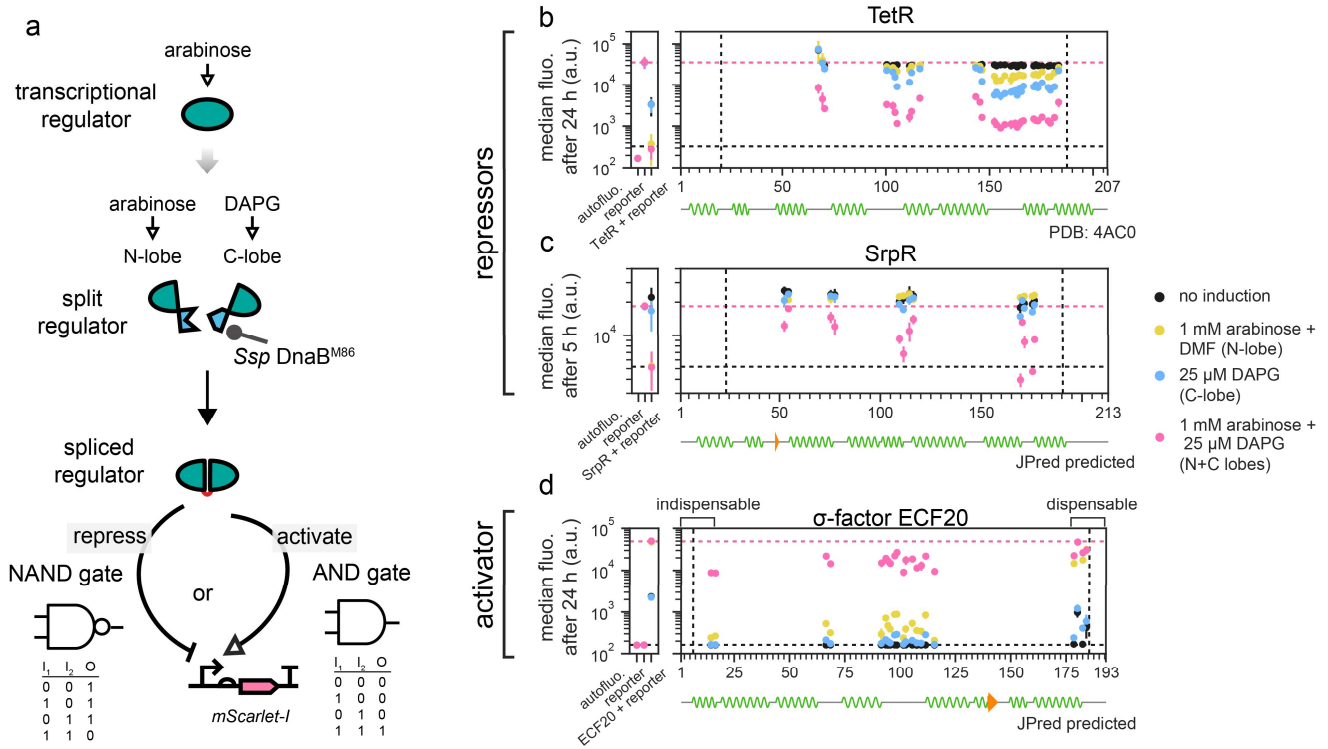


**Fig. 2 IBM as a universal method to exhaust split sites for AND and NAND logic gate engineering.** **a.** Any transcription factor with a function that can be wired to an assay-friendly output could be subjected to IBM for logic gate engineering. **b-d.** Intron-bisection maps for TetR (**b**, 3 seams identified), SrpR (**c**, 4 seams), and ECF20 (**d**, 3 seams). Split clones of TetR and SrpR (or ECF) achieved major off (or on) activities when both the N- and C-lobes were present.  $\bar{y}$  locations and error bars are mean and std of median fluorescence from experiments performed on 3 different days. Vertical dashed lines bound the permitted transposition window and horizontal dashed lines bound the ranges of activities that could be attained by the split proteins. **d.** By-products of IBM revealed a truncatable region of ECF20 which when removed did not adversely affect activation. **b-d.** See **Supplementary Fig. 6-8** for site distributions and activities at 5 h (TetR and ECF20) and 24 h (SrpR). See **Supplementary Fig. 9** for explanations of controls (leftmost subplots).

## 169 **IBM expands the range of split sites discoverable in TetR**

170 Previously reported approaches in bisection mapping for logic gates engineering utilized protein-protein  
171 interacting domains like the SYNZIPs as fusion partners<sup>30</sup>. We hypothesized that inteins make a better  
172 choice because they would be excised from the splice product, whereas additional domains could exert  
173 steric hindrance, especially when the host protein function requires multimerization or interactions with  
174 other proteins. To test our hypothesis, a representative site from each split seam identified on split TetR  
175 was selected and the split M86 intein was replaced by SYNZIPs in a similar manner as above (**Fig. 3a**). Of the  
176 three tested sites, site 166/167 showed a stronger level of repression (~ 4 fold) compared to the other two  
177 (~ 2 fold), despite having the least possible amount of reconstituted protein (**Supplementary Fig. 15**). The  
178 differences in repression strengths between split sites, when SYNZIPs were used, demonstrated their  
179 differential tolerances towards additional domains. Whereas in IBM, all three sites showed good levels of  
180 repressions that were strong enough to be identified from a single screen. Hence, the use of an intein could  
181 enable split sites that might be inaccessible by protein-protein interacting domains and expands the range  
182 of split sites that could be identified for logic gate engineering.

## 183 **IBM revealed limitations in inferring split sites from secondary structure alignment**

184 When choosing split sites for a new protein from a known protein family, a conventional approach is to  
185 align the sequences and their predicted secondary structures, and find common loops between  
186 homologous structures to identify putative split sites<sup>44</sup>. Upon the completion of the intein-bisection maps  
187 of TetR and SrpR, we realized our data might shed light on how reliable the approach is, and therefore  
188 aligned the two protein sequences by secondary structures<sup>45</sup> along with the identified split sites (**Fig. 3b**,  
189 **Supplementary Fig. 16**). The alignment indicated that only two split seams are shared between TetR and  
190 SrpR. Sites on seam 2 of TetR and seam 3 of SrpR were not aligned and would be overlooked if the  
191 alignment approach were taken. Likewise, on SrpR split sites were found on the loop that demarcates the  
192 DNA binding domain from the dimerization domain, but those sites would be unexpected if TetR served as  
193 the reference model. Our results therefore suggest the secondary structure alignment approach works but  
194 could miss other potentially useful split sites, which could be discovered by IBM.

## 195 **Mitigation of undesirable basal activities in highly active proteins through IBM**

196 Splitting highly active proteins could suppress their background activities. This was best illustrated by the  
197 IBM generated split  $\beta$ -lactamases (**Fig. 3c**). When the full CDS of  $\beta$ -lactamase was placed under the control  
198 of  $P_{araBAD}$ , the hosting bacteria could grow in ampicillin regardless of arabinose addition, proving that leaky  
199 expression of  $\beta$ -lactamase was sufficient to confer resistance. In contrast, split  $\beta$ -lactamases did not lead to  
200 cell growth if inducers were absent. This tightening of protein expression control could also be concluded  
201 from further analyses of single-cell fluorescence data from **Fig. 2**. Intact TetR and SrpR had stronger  
202 repression than their bipartite counterparts at 5 h. At 24 h, however, in the absence of induction the  
203 fluorescence of unrepressed cells was much lower (**Fig. 3c, Supplementary Fig. 17**). Whereas, many  
204 bipartite repressors at 24 h had higher unrepressed fluorescence, better separation of populations  
205 between on and off states and hence high fold changes. This phenomenon was even more pronounced on  
206 the ECF20 activator – at 5 h, basal activities already gave a strong off-state fluorescence and four split  
207 constructs started to benefit from fold change improvement, and at 24 h the average fold change of the  
208 worst performing split ECF20 construct was around 54 compared to 22 of the intact ECF20 (**Supplementary**  
209 **Fig. 17**). These data from  $\beta$ -lactamase, repressors and activators implied that intact proteins had  
210 accumulated over time due to leaky expression from a single promoter, but when they were split by IBM  
211 and placed under independent promoters, the conferred AND logic led to a lower probability of assembling  
212 a functional protein, thereby reducing the overall undesirable basal activities at the off states.



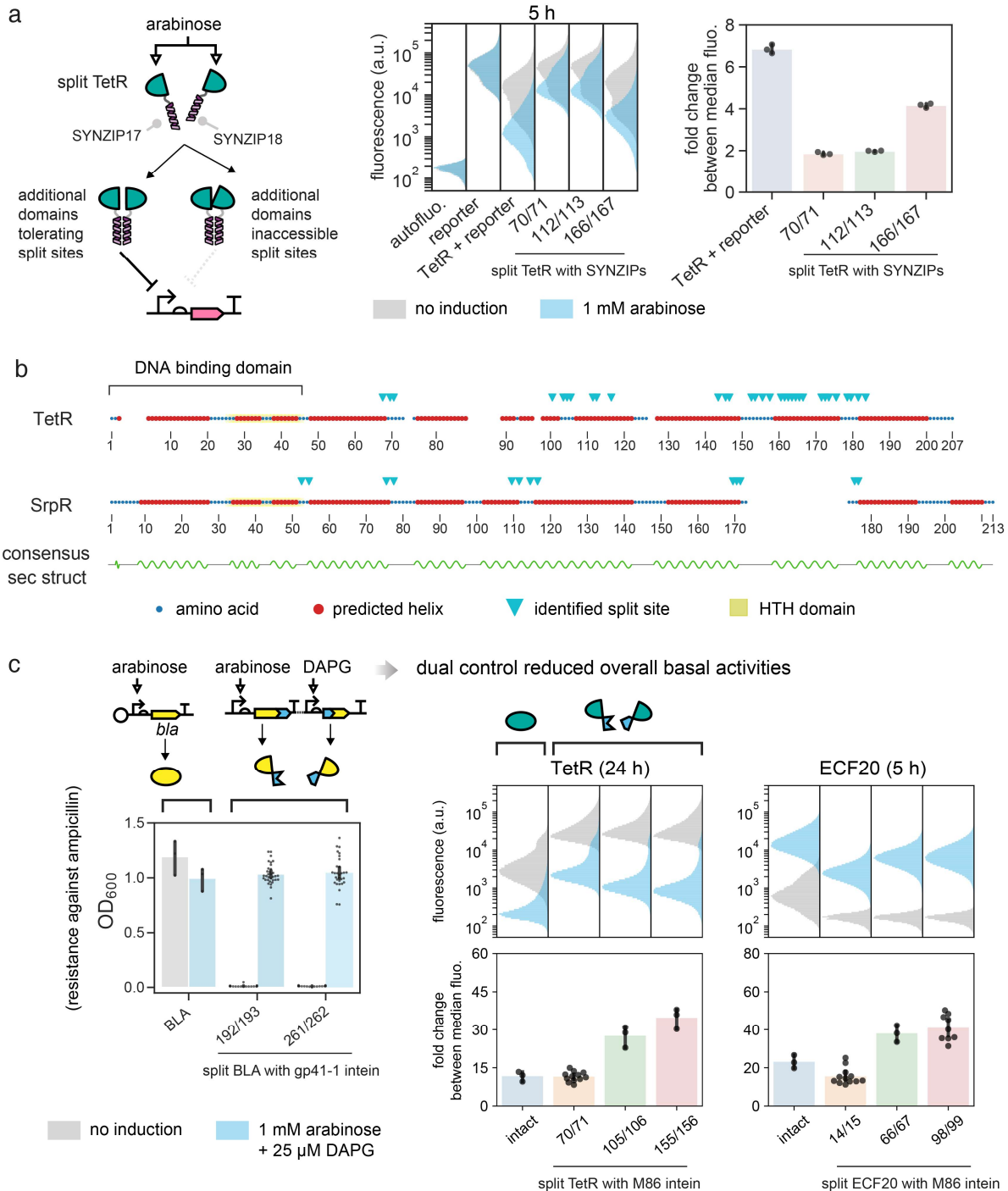


**Fig. 3 Benefits of IBM and reduction of basal activities by IBM. a.** Substitution of the split M86 intein inserted in split TetR by SYNZIP. Representative sites were chosen within the 3 identified split seams. Results showed different split sites had differential tolerances towards additional protein domains, but all split sites functioned well when the intein was used (**Fig. 2b**). Single-cell fluorescence values were pooled from 3 biological replicates. **b.** IBM-identified split sites of homologous TetR and SrpR do not necessarily map to loops between consensus helical domains, highlighting the limitation of guessing split sites for a new protein by secondary structure alignment. **c.** Splitting highly active proteins can reduce their basal activities. Left panel: leaky expression of BLA led to ampicillin resistance in absence of induction, which could be improved by splitting BLA. Middle and right panels: Fluorescence distributions and fold changes between fully on and fully off states of intact and split TetR and ECF20 were shown. Representative sites were chosen from each identified seam. In most cases the split clones had lower basal activities and therefore larger fold changes between on and off states. **b-c.** Data reused from Fig. 2 and Supplementary Fig. 8 but further analyzed. **a, c.** Single-cell fluorescence values were pooled from experiments performed on 3 different days. In fold change calculations, bar heights and error bars represent mean and std.

213 **Transposon-mediated engineering of post-translational inducibility into inteins to control protein**  
214 **function**

215 In theory, our IBM workflow should allow one to use a conditional intein<sup>46-48</sup> in place of a split intein, and  
216 then screen for insertion or split sites that would enable post-translational control of protein function. We  
217 thus synthesized and tested three reported chemogenic conditional inteins<sup>49-51</sup> from the literature, but they  
218 did not work well under our specific context (**Supplementary Fig. 18**). Given the circumstances we decided  
219 to take a different approach and asked whether we could create inducible inteins de novo, by transposing  
220 drug-controlled domains into the M86 intein. We reasoned that a conversion of the spontaneous split  
221 intein into a conditional one would allow us to exert control over protein activity through addition or  
222 removal of small molecules (**Fig. 4a**). To do so, we synthesized the ligand binding domain of human  
223 estrogen receptor (ER-LBD)<sup>29</sup> and the camelid anti-caffeine VHH (acVHH) antibodies<sup>52, 53</sup>. For the former, we  
224 hypothesized that similar to the previous study, possible insertion sites exist within the cis-intein, where  
225 intein folding would be obstructed by the interrupting ER-LBD until 4-hydroxytamoxifen (4-HT) binding  
226 elicits a structural change that relieves the effect. For the latter, we hypothesized that at certain split sites,  
227 the split intein lobes would suffer from reduced interacting surfaces and hence diminished affinities for  
228 spontaneous assemblies, but could be rescued by an externally supplied source upon ligand-induced  
229 dimerization of acVHH.

230

231 **Engineering a 4-HT-inducible mCherry by domain-insertion mapping**

232 In our first example we aimed to control splicing and fluorescence of split mCherry using a slightly modified  
233 version of domain-insertion profiling. We first inserted the cis-M86 intein between amino residues 192 and  
234 193 of mCherry since this mCherry split site performed well in the fluorescence complementation  
235 experiment (**Fig. 1d**) and was at the center of the flexible loop. We then performed the domain-insertion of  
236 the ER-LBD into the cis-M86 intein, now between mCherry(1-192) and mCherry(193-236), via random  
237 transposition, and then replaced the min Mu-transposon by the CDS of the ER-LBD domain (**Fig. 4b**). We  
238 induced protein expression by the addition of arabinose, performed a series of positive and negative cell  
239 sorting with or without 4-HT, obtained individual strains, characterized and then sequenced them. Of the 7  
240 insertion sites identified, none yielded any activities at 5 h post-induction (**Supplementary Fig. 19**), but  
241 differential responses between 4-HT-uninduced and induced states could be observed at 24 h. Some  
242 recovered sufficiently high fluorescence comparable to the intact M86 intein but not without sacrificing  
243 basal activities.

244 We then selected three representative sites that spanned the activity ranges and proceeded to verify dose-  
245 dependent activities. Cells were subjected to a gradient of 4-HT induction and harvested for fluorescence  
246 and protein content analysis (**Fig. 4c**). All three strains showed gradual upshift of fluorescent populations as  
247 4-HT concentration increased. Similarly, a Western blot of whole-cell lysates also indicated a 4-HT-  
248 dependent increase in spliced mCherry formation, even though most precursors did not undergo splicing  
249 regardless of split sites or inducer concentrations. The exception is the strain where ER-LBD was inserted at  
250 site 77/78 within the M86 intein, in which the bands of the spliced products were too weak to be detected,  
251 and the band for the spliced products under 10  $\mu$ M 4-HT was barely visible. The Western blot also  
252 confirmed the existence of spliced mCherry in the absence of 4-HT and explained the strong basal  
253 fluorescence of the inserted clones.

254 We further asked whether the novel conditional inteins are transferrable to another host protein, and so  
255 cloned all seven ER-LBD-inserted inteins into the identified site 101/102 of ECF20. Clones were subjected to  
256 either 0 or 10  $\mu$ M 4-HT induction under various arabinose concentrations (**Supplementary Fig. 20**). In the  
257 best-case scenario, strain 76/77 under 0.0625 mM arabinose yielded a small but statistically significant  
258 increase in fluorescence when 4-HT was added. Nevertheless, spontaneous splicing already generated

259 sufficient amount of spliced ECF20, which were high active and resulted in strong basal activities, and  
260 rendered the circuit impractical for further use.

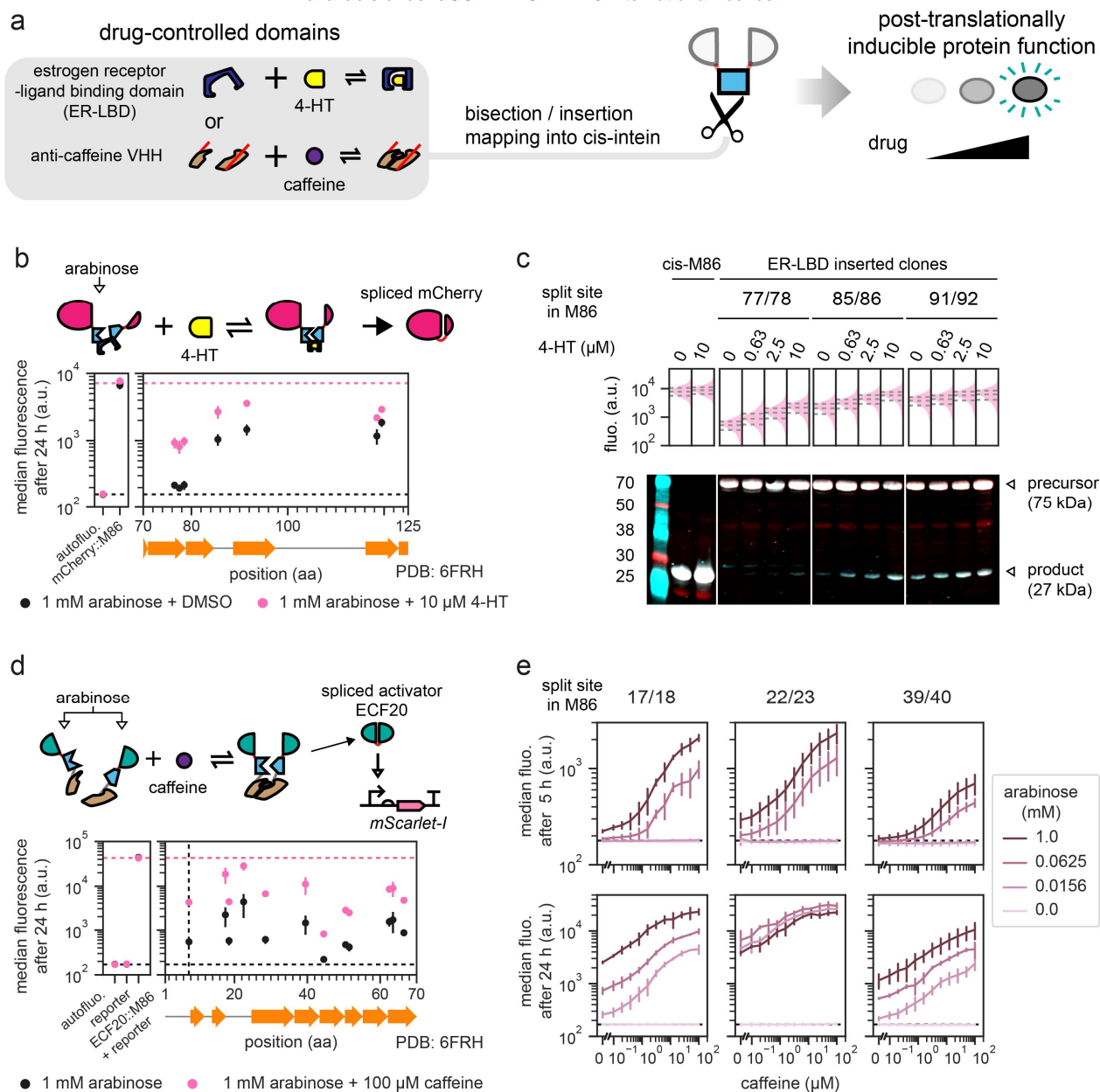


**Fig. 4 Transposon as a tool to engineer inducibility into an intein for protein function control.** **a.** The M86 intein in its cis-form can be inserted in an identified split site within the protein of interest, and then bisected or inserted with drug-controlled domains, which leads to inducible splicing and inducible function of the host protein. **b.** 7 insertion sites identified via domain-insertion mapping of the estrogen receptor-ligand binding domain into the M86 intein within mCherry interrupted at 192/193, where addition of 4-HT led to increased fluorescence. **c.** Selected clones from (b) showed gradual increase in fluorescence and spliced product formation as the concentrations of 4-HT increased, despite the fact that most precursors were unspliced. Single-cell fluorescence values were obtained from one biological sample. Interquartile ranges are denoted by horizontal dashed lines. mCherry N-lobes were labelled in red and C-lobes were labelled in turquoise, and their superpositions give a white color. **d.** 11 split sites for anti-caffeine VHH identified on the M86 intein that interrupted the activator ECF20 at 101/102. In those clones, addition of caffeine led to increased activation activities. **e.** Selected clones from (d) had increased activation activities as caffeine concentration increased, and leakiness due to spontaneous assembly could be mitigated by lowering the total split protein concentrations. **b, d.** Each vertical group of spots represents an identified insertion/split site, aligned to the M86 intein secondary structure. See **Supplementary Fig. 19, 22** for site distributions and activities at 5 h. **b, d, e.** y locations and error bars are mean and std of median fluorescence from experiments performed on 3 different days. Horizontal dashed lines bound the maximum (b and d only) and minimum fluorescence that could be achieved by the split or inserted constructs.

## 261 **Engineering caffeine-inducible activation by acVHH-assisted bisection mapping**

262 In the second example of post-translational inducibility engineering we generated a caffeine-inducible  
263 activation by transposing two acVHH domains, each with a 10-residue linker, into the cis-M86 intein at site  
264 101/102 of ECF20. Consequently, the intein was split and the resulting split protein parts were then placed  
265 under the control of two arabinose inducible promoters, one for the N-lobe and another for the C-lobe,  
266 simplifying the effort to tune protein expression strengths. Prior to the bisection mapping experiment, we  
267 established comparable performance between caffeine-inducible dimerization and the rapamycin-inducible  
268 FRB/FKPB dimerization in reconstituting an evolved split T7 RNA polymerase<sup>54</sup> (**Supplementary Fig. 21**).  
269 FRB/FKBP had lower propensity to self-associate without ligand but we chose acVHH since caffeine is  
270 inexpensive.

271 We then carried out the acVHH-assisted bisection mapping on the M86 intein, following a similar workflow  
272 as we did for the domain-insertion mapping of ER-LBD. 12 split sites close to the M86 N-terminus were  
273 identified and they had increased fluorescence when cells were grown under 100  $\mu$ M caffeine for 24 h  
274 when compared to the lack of caffeine induction (**Fig. 4d, Supplementary Fig. 22**). Again, all strains had  
275 either strong basal and strong maximum activities or weak activities for both states. Among them, three  
276 strains displayed discernable differences in fluorescence at 5 h and thus were subjected to tests for dose-  
277 dependent activation.

278 From previous literature and the experiment on split T7 RNA polymerase we were cognizant that  
279 spontaneous assembly positively correlated with intracellular protein concentrations and could be  
280 mitigated by tuning down protein expression. We therefore grew the three strains in a 2-dimension  
281 gradient of caffeine and arabinose, and characterized their fluorescence at 5 and 24 h (**Fig. 4e,**  
282 **Supplementary Fig. 23**). Activation was an increasing function of caffeine and to some extent the response  
283 resembled a hill-curve. Apart from site 22/23 at 24 h post-induction, reducing arabinose concentration  
284 could reduce leaky activation at the expense of the overall activities. We then attempted to test those  
285 inducible inteins' transferability, by cloning them back into mCherry split at 192/193 for fluorescence and  
286 Western blot assays, but neither showed any signs of splicing (**Supplementary Fig. 24**). We speculated the  
287 splicing efficiencies under caffeine induction were too low and only worked with ECF20 given its extreme  
288 potency in activation.

289 The examples of transposing ER-LBD and acVHH into a spontaneously splicing intein generated prototypes  
290 of inducible inteins with admittedly limited performance and transferability, but they were only the first  
291 steps. With these two examples we proved in principle, there exists a systematic approach to introduce  
292 inducibility into an intein, and hence into a protein of interest, provided that its function could be screened  
293 conveniently.

## 294 **Discussion**

295 We have established IBM as a useful tool for split protein-intein engineering. Thus far we have only  
296 employed the *Ssp* DnaB<sup>M86</sup> and the gp41-1 intein. Repeating our IBM experiments using different split  
297 inteins may reveal even more split sites at new positions, since extein junctions with different amino acid  
298 compositions and lengths would be incorporated. This may alter the rigidity of the resulting linkers and  
299 hence functionalize other unprobed split sites. If shorter linkers are desired, a "promiscuous" intein<sup>55</sup> could  
300 be helpful, since a designated +2 extein residue could be omitted and supplied by the host protein.

301 The computational method by Palanisamy et al<sup>25</sup>, and the SPELL algorithm<sup>26</sup>, both mentioned above,  
302 suggest split sites based on protein 3D structures and works in silico, whereas our IBM/acVHH-assisted BM  
303 workflow takes on an empirical approach and addresses the same issue with different constraints.  
304 Sometimes solved 3D structures may be unavailable and de novo structure prediction might not sufficiently  
305 reflect the multimerization required in some proteins like TetR. Conversely, IBM/acVHH-assisted BM  
306 requires the protein function to be manifested as an easily screen-able output and would be tremendous

307 difficulty or outright impossible if the function of interest is, for example, chemotaxis. It also requires a  
308 chassis capable of creating a complex library through highly efficiently transformation, and so for the time  
309 being it only applies to bacteria or yeasts. These limitations are absent in computational methods for split  
310 site predictions, however. Furthermore, data from IBM/acVHH-assisted BM may be fed back into and refine  
311 those algorithms. We therefore advocate IBM/acVHH-assisted BM not as a competitor, but rather, a  
312 complement to the computation approaches.

313 In this work we created two novel inducible variants of the M86 intein. At the current stage, these two  
314 inteins have limited dynamic ranges and strong spontaneous splicing activities, and thus are specific to their  
315 protein contexts where they were screened. Therefore, our work was a proof of concept, and only the first  
316 step towards a systematic approach in converting spontaneously splicing inteins to conditional ones. So far  
317 only the M86 intein was tested as the engineering precursor. Other inteins standardized by our group lately  
318 might lead to conditional inteins with better on-off characteristics. There are also other synthetic ligand  
319 binding domains, for example, uniRapR<sup>56</sup> and iFKBP/FRB<sup>57</sup> that are potential replacements for ER-LBD and  
320 acVHH. Given so, the performance of any inducible intein engineered through this method may depend on  
321 complex interactions between the intein of choice, the drug-responsive domain, and the insertion/split  
322 positions. Each could influence the other two factors. Hence, future efforts in engineering more inducible  
323 inteins would likely require a combinatorial exploration of all three factors to identify the optimal structure  
324 drug-induced protein splicing.

325 The limited performance of the two inducible intein from this study could also be improved via directed  
326 evolution<sup>23, 32, 49, 58, 59</sup>, which can mutate these inteins such they splicing with better efficiencies and with  
327 lower basal activities, and allow them to perform sufficiently well when inserted into other host proteins.  
328 We foresee a powerful combination between domain-insertion/acVHH-assisted bisection mapping and  
329 directed evolution, where the former identifies the optimal sites for differential activities. The sites can  
330 then be exploited by the latter which often requires differential responses to prime the evolution process.  
331 This should create more inducible inteins which would be valuable tools when additional domains on a  
332 protein cannot be tolerated (**Supplementary Fig. 25**).

333 Our IBM workflow employed random transposition to diversify DNA insertion. This method has known  
334 issues including sequence bias<sup>60-64</sup> and inexhaustive space search<sup>28, 29, 64, 65</sup>. Despite so, in our final libraries  
335 prior to screening, sequenced by Next Generation Sequencing (NGS), we obtained at least 87% coverage on  
336 possible amino acid split / insertion positions (**Supplementary Fig. 26, Supplementary Table 1**), which  
337 sufficiently explored the sequence space. If unbiased and full position coverage is desired, the step of  
338 random transposition could be replaced by the recently developed Saturated Programmable Insertion  
339 Engineering (SPINE)<sup>64</sup>, which hardcodes all insertion possibilities into oligonucleotide pools. Incorporation  
340 of SPINE into the IBM workflow would return bisection / insertion maps with even higher confidences.

341 In summary, we presented a robust method to screen and identify protein split sites for the insertion of a  
342 split intein. We have recently characterized a library of orthogonal split inteins<sup>16</sup>. With the help of IBM, a  
343 large number of orthogonal AND or NAND gates could be created in a streamlined fashion, expediting the  
344 development of biocomputing units. Moreover, we demonstrated in principle that transposing drug-  
345 controlled domains could create inducible inteins to control host protein function post-translationally.  
346 Together, they constitute an empirical and systematic approach towards split protein and protein function  
347 control engineering, and should benefit general biologists who seek to use inteins on split proteins.

348

## 349 **Methods**

### 350 **Strains, media, and inducers**

351 *Escherichia coli* TOP10 (Invitrogen) was used for routine cloning. For all bisection/insertion mapping, the  
352 first insertion libraries were always transformed into the electrocompetent *E. coli* NEB 10-beta (C3020K,  
353 NEB). For the rest of the workflow the strain was switched back to TOP10. The only exception was the IBM  
354 experiment on mCherry and its outcome simulation experiment, where NEB 10-beta was used in all steps.  
355 All strains were grown in the Miller's Lysogeny Broth (LB, 10 g/L tryptone, 5 g/L yeast extract, 10 g/L sodium  
356 chloride) in liquid medium or agar supplemented with the appropriate antibiotics (unless noted otherwise)  
357 at the final concentrations of: kanamycin (K4000, Sigma-Aldrich), 50 µg/mL; chloramphenicol (C0378,  
358 Sigma-Aldrich), 25 µg/mL; ampicillin (A9518, Sigma-Aldrich), 100 µg/mL; tetracycline (T8032, Sigma-  
359 Aldrich), 10 µg/mL, spectinomycin (ab141968, Abcam), 50 µg/mL.

360 For preparation of stock inducers, powder of L-(+)-Arabinose (A3256, Sigma-Aldrich, 1 M), N-(3-  
361 Oxohexanoyl)-L-homoserine lactone (AHL, K3007, Sigma-Aldrich, 25 mM), or caffeine (A10431.22, VWR, 10  
362 mM) was dissolved in water; 2,4-Diacetylphloroglucinol (DAPG, 16345, Cambridge BioScience, 25 mM), in  
363 dimethylformamide (D4551, Sigma-Aldrich); Rapamycin (S1039-SEL, Stratech, 10 mM), (Z)-4-  
364 hydroxytamoxifen (4-HT, H7904, Sigma-Aldrich, 10 mM), 3,3',5-triiodo-L-thyronine (T<sub>3</sub>, HY-A0070A,  
365 Cambridge BioScience, 10 mM) in dimethyl sulfoxide (D8418, Sigma-Aldrich), with the stock concentrations  
366 denoted in brackets. For inductions involving inducers dissolved in organic solvents, the volumes of inducer  
367 were less than or equal to 1% of the final volume.

### 368 **DNA assemblies and purification**

369 Synthetic DNA constructs were built using Gibson Assembly, Golden Gate Assembly and conventional  
370 subcloning using restriction digestion and ligation, with the method chosen depending on their individual  
371 needs. Whenever necessary, synonymous mutations were introduced to remove internal BsaI, BbsI or SapI  
372 restriction sites. Standard molecular biology protocols were observed. The ZymoPURE II Plasmid Midiprep  
373 Kit (D4200, Zymo) was used for DNA library extractions. For the purification of DNA, the Monarch Nucleic  
374 Acid Purification Kits (T1020 and T1030, NEB) were used. All restriction enzymes and ligases were bought  
375 from NEB. MuA protein was purified in collaboration with Domus Biotechnologies (Turku, Finland)  
376 essentially as described<sup>66</sup>.

### 377 **Cell growth for fluorescence assays and OD measurements**

378 Cells were routinely cultured in 96-well plates (655096, Greiner Bio-One) sealed with breathable  
379 membranes (Z380059, Sigma-Aldrich), and incubated at 37 °C in plate shakers (AS-03020-00, Allsheng) with  
380 1000 rpm orbital shaking motion. An assay of synthetic constructs began with an inoculation of a single  
381 colony from an agar plate into a well with 200 µL of medium, which was then grown for 16-18 h. The next  
382 day, 2 µL of the overnight culture was diluted 1:100 into 198 µL of fresh medium with or without inducers  
383 and grown for 5 h. The membrane was then removed and 2 µL of the culture was sampled. A new seal was  
384 applied, and the plate was returned to the shaker to further grow until the total time of inoculation was 24  
385 h. Afterwards, 2 µL (5 h) or 0.5 µL (24 h) of the culture was sampled. Changes to growth time were noted in  
386 individual figures where appropriate. Exception to the above applies to the split mCherry splicing  
387 experiment, the mCherry BiFC experiment and the split TetR-SYNZIP experiment, where overnight cultures  
388 were diluted 1:100 into 1mL of fresh medium in 96-deepwell plates (E2896-2110, Starlab). For the assays of  
389 strains identified from bisection/insertion mapping experiments, the overnight culture was inoculated from  
390 the saved glycerol stocks (described below). Assays measuring resistance against ampicillin were performed  
391 in a similar manner, the only difference was that ampicillin was added at the same time as inducers, and  
392 growth was only measured after 24 h.

393

## 394 **Optical density measurements by plate reader**

395 End-point optical densities at 600 nm (OD<sub>600</sub>) were measured with a FLUOstar Omega plate reader (BMG  
396 Labtech). The software Omega Control v5.11 (BMG Labtech) was used for data acquisition and Omega  
397 MARS v3.32 (BMG Labtech) was used for data export. The optical densities of blank wells from the same  
398 plate were subtracted from all other wells.

## 399 **Fluorescence measurement by flow cytometry**

400 Prior to analysis, sampled cultures were diluted into 1× phosphate-buffered saline (K813-500ML, VWR) with  
401 2 mg/mL kanamycin to a total volume of 200 µL. Diluted cells sampled at 5 h were incubated at 4 °C for a  
402 minimum of one hour to promote fluorophore maturation, whereas those at 24 h were directly assayed.  
403 Cells were passed into the Attune NxT Flow Cytometer (Thermo Fisher) equipped with the Autosampler for  
404 analysis. For each well, 100 µL of diluted cells were run at 500 µL/min and at least 10<sup>5</sup> events were  
405 recorded. Red fluorescence was acquired on the YL2-H channel (excitation 561 nm, emission 615/25 nm).  
406 Exported FCS files were processed using an in-house Python script dependent on the FlowCytometryTools  
407 package v0.5.0. All samples were gated on FCS-H, FCS-A, SSC-H and SSC-A for events between 10<sup>3</sup> – 10<sup>5</sup>  
408 arbitrary units, followed by gating on YL2-A and YL2-H between 1 to 10<sup>6</sup> arbitrary units.

## 409 **Transposition and bisection/insertion library preparations**

410 The mini-Mu transposon used in this study was modified from the one used by Segall-Shapiro et al.<sup>27</sup> with  
411 BbsI and SapI sites incorporated into the R1 recognition sites. Prior to transposition the transposon was  
412 released from its host vector by restriction digestion using BglII followed by purification from agarose gels.  
413 The coding DNA sequence of interest was trimmed at the N- and C- termini before being subcloned into a  
414 staging vector. In vitro transposition reaction was set up following an established protocol<sup>67</sup> with slight  
415 customization: 150 ng of the staging plasmid and 150 ng transposon were mixed with 660 ng of MuA. For  
416 each insertion library 5-6 reactions of 25 µL each were prepared and incubated at 30 °C in a thermocycler  
417 for 6 h, followed by heat inactivation at 80 °C for 10 min. All reactions were pooled, purified, and then  
418 eluted in 10 µL of nuclease-free water. The resulting DNA was then electroporated into a total of 200 µL of  
419 NEB 10-beta cells in four separate cuvettes and recovered following manufacturer's protocol. Then, 10 µL  
420 of the recovered cells (~ 2 mL) were removed, serially diluted into 0.85% sodium chloride (w/v) and spread  
421 onto LB agar with kanamycin and chloramphenicol for colony counting. The library coverage was defined as  
422 the total number of obtainable transformants / (size of staging plasmid in bp × 2) and were at least 20-fold  
423 for all experiments. Libraries that did not meet the criteria were discarded and transposition reactions were  
424 repeated. For libraries with sufficient coverage, the rest of the recovered cells were spread onto LB agar.  
425 Bacterial lawns were then washed down by 0.85% sodium chloride and a small aliquot was saved as a  
426 glycerol stock. The rest were pelleted, and the DNA was extracted by midiprep.

427 10 µg of the midiprep DNA from the initial insertion library was digested by BsaI and then resolved on  
428 agarose gels until bands were well-separated. The band corresponding to the trimmed coding DNA  
429 sequences with insertions was then excised, purified, and ligated to the linearized expression vector in 1:2  
430 molar ratio for insert:vector. The overnight ligated product was then purified and electroporated into 100  
431 µL of in-house-prepared electrocompetent cell, which were recovered in 2 mL SOC for 1 h, concentrated  
432 and then spread onto LB agar and grown overnight. Library coverage estimation and DNA extraction of the  
433 library were performed similar to that in transposition, except that the size of the insertable positions  
434 equals to the size of trimmed coding DNA sequence in bp. At this stage library coverages were typically >  
435 500-fold.

436 To replace the inserted transposon with split inteins or drug-controlled domains, 60 ng of the midiprep  
437 DNA from the open reading frame (ORF) insertion library was mixed with substitution inserts (released  
438 from the cloning plasmids) in a 1:5 molar ratio for plasmid:insert, and added to a Golden Gate reaction  
439 mixture<sup>68</sup> with 20 units of BbsI, 10 units of SapI and 400 units of T4 DNA ligase. The reaction was then run in



440 a thermocycler with the following program: (37 °C for 3 min, 16 °C for 4 min) × 25 cycles, 37 °C for 30 min,  
441 and 65 °C for 20 min. Usually 5-6 reactions were run, pooled, purified and electroporated into 100 µL of in-  
442 house-prepared electrocompetent cells. Electrocompetent cells carried a reporter plasmid wherever  
443 required. Cells were recovered and the library coverage estimation was performed in the same manner as  
444 the preparation of the ORF insertion library. At this stage library coverages were typically > 100-fold.

#### 445 **Library screening**

446 For IBM on mCherry, recovered cells from the final library were first induced with both arabinose and AHL,  
447 and sorted by fluorescence activated cell sorting (see below). Retrieved cells were then spread onto LB agar  
448 for colony picking. For IBM on β-lactamase, recovered cells from the final library were first induced with  
449 arabinose and DAPG overnight, the culture was then diluted 1:100 in fresh medium containing arabinose,  
450 DAPG and ampicillin, and was grown for another overnight. The resulting culture was serially diluted onto  
451 solid medium with inducers and ampicillin for isolating single colonies. For IBM on TetR, SrpR and ECF20,  
452 recovered cells from the final library were serially diluted such that single colonies could be observed when  
453 they were spread onto LB agar with arabinose and DAPG. For TetR and SrpR, functional reconstitution of  
454 the bipartite protein represses expression of mScarlet-I and therefore yielded visibly white or pale pink  
455 colonies. The opposite was true for ECF20. These colonies were picked directly. For the M86 intein inserted  
456 with ER-LBD or the M86 intein bisected by acVHH, recovered cells from the final library were first induced  
457 with arabinose and 4-HT or caffeine. They were then sorted for populations with fluorescence higher than  
458 the library without 4-HT or caffeine induction (positive sort). Sorted cells were regrown in the presence of  
459 arabinose only and then sorted for populations with lower fluorescence (negative sort). The positive sort  
460 was repeated once, and the retrieved cells were spread onto LB agar to obtain single colonies for picking.

#### 461 **Fluorescence activated cell sorting (FACS) experiment**

462 For the initial sort, 100 µL of the library was inoculated into 25 mL of medium with inducers and grown  
463 overnight for 18 – 24 h. The next day, 10 µL of the culture was diluted into 10 mL 1× phosphate-buffered  
464 saline and then passed into the cytometer. Cell sorting was performed on a FACS Aria II cytometer (BD-  
465 Biosciences) through the red fluorescent channel (excitation 561 nm, emission 610/20 nm), under the  
466 Purity Mode. Cells were first gated on irregularly shaped FSC-A and SSC-A gates to exclude non-cellular  
467 materials, and then gated on boundaries defined by the previous libraries with or without induction. Gate  
468 sizes and positions were tailored to individual experiments. Typically, 0.5 – 1 million gated events were  
469 collected into a 15 mL conical tube with 5 mL of LB supplemented with 1 % D-Glucose (10117, VWR) and  
470 without antibiotics. Collected cells were recovered for 2 h at 37 °C with 160 rpm shaking. Then, the volume  
471 was topped to 15 mL using LB with the next set of inducers and grown overnight for 16-18 h for the next  
472 sorting experiment. After the final cell sorting, the overnight culture was diluted and plated onto LB agar to  
473 obtain single colonies for strain isolation.

#### 474 **Candidate strain isolation, characterization and split/insertion site mapping**

475 In most cases > 500 single colonies with desirable traits were individually picked into 96-well plates with  
476 200 µL of LB medium for 16-18 h of growth, which were subjected to 16-24 h of induction assays to look for  
477 AND logic (mCherry, β-lactamase and ECF20), NAND logic (TetR and SrpR), or differential expression (with  
478 the M86 intein inserted or bisected). The fluorescence of the candidate clones was then measured on the  
479 FLUOstar Omega plate reader (BMG Labtech) and ranked. The best clones with desirable traits (~96 for IBM  
480 and ~40 for M86 intein engineering) were isolated with assistance from an OT-2 robot (Opentrons). The  
481 shortlisted clones were saved as temporary glycerol stocks and then subjected to fluorescence assays as  
482 described above for proper characterization, which generated the data for plotting the bisection/insertion  
483 maps. Strains that showed strong experiment-to-experiment variations in fluorescence were excluded for  
484 further use. A small aliquot of each cell strain in liquid suspension was then subjected to polymerase chain  
485 reactions (PCR), which amplified the N-terminal (mCherry) or the C-terminal (all others) joints. The PCR  
486 products were purified and sent for Sanger sequencing. Poor sequencing results or reads that suggested

487 non-single clones were discarded. The rest of the sequencing results were analyzed with a customized  
488 Python script utilizing the Biopython package v1.76<sup>69</sup> to deduce split or insertion sites by local alignment of  
489 sequences. Sites were mapped back to their fluorescence profiles and protein secondary structures  
490 (rendered using the Biotite package v0.20.1<sup>70</sup>).

#### 491 **SDS-PAGE and Western blots for whole-cell lysate analysis**

492 Cells cultured for Western blots were grown in 30 mL universal tubes (E1412-3011, Starlab) placed inside a  
493 shaker (Infors HT) maintained at 37 °C, 160 rpm. For each sample, a single colony was inoculated into 2 mL  
494 of medium and grown for 16-18 h. The next day, the overnight culture was diluted 1:100 into 2 mL of fresh  
495 medium with the appropriate inducers and grown for 24 h unless specified otherwise. Then, where  
496 appropriate, 0.5 µL of culture was removed for fluorescence measure for flow cytometry, with the pre-lysis  
497 fluorescent distributions displayed in the same figure. For detection of protein expression, in most cases 1  
498 mL of culture was harvested. Exception to the above applies to the split mCherry-split M86 intein splicing  
499 experiment, the mCherry BiFC experiment and the split TetR-SYNZIP experiment, where the volumes of  
500 bacterial culture harvested were adjusted by optical densities to standardize the amount of cellular  
501 materials used in cell lysis. Bacterial cells were centrifugation at 17, 000 × g and resuspended in 50 µL of 1×  
502 Laemmli sample buffer (1610747, Bio-Rad), boiled at 100 °C for 10 min, and centrifuged at 17, 000 × g for  
503 10 min. 5 or 10 µL of the supernatant were resolved on an Any kD TGX Stain-Free protein gel (4568126, Bio-  
504 Rad) alongside a Chameleon Duo Pre-Stained Protein Ladder (928-60000, Li-cor). Protein contents were  
505 then transferred to a nitrocellulose membrane (1704270, Bio-Rad) through a semi-dry transfer protocol  
506 (1704150, Bio-Rad). The manufacturer's protocol (Doc. #988-13627, Licor) was followed for blocking,  
507 antibody incubation, washing and detection of near-infrared probes on secondary antibody. We used 5%  
508 (w/v) skimmed milk in 1× tris-buffered saline (1706435, Bio-Rad) as the blocking reagent. The mCherry  
509 constructs involved in the Western blot assays carried a hexahistidine tag at the C-terminus and an epitope  
510 (residues 27-41) exists within the N-lobe. Bipartite proteins were detected using the rabbit anti-mCherry  
511 (A00682, GenScript, 1:3000 diluted), the mouse anti-His (A00186, GenScript, 1:5000 diluted), and the rabbit  
512 anti-HA (902303, Biologend, 1:1000 diluted) antibodies. They reacted against the IRDye 680RD goat anti-  
513 rabbit (925-68071, Licor) or the IRDye 800CW goat anti-mouse (925-32210, Li-cor) secondary antibodies,  
514 both diluted at 1:20,000. Membrane imaging was performed on the Odyssey CLx Infrared Imaging System  
515 (Li-cor) and the resulting images were processed using Image Studio Lite v5.2.5 software (Li-cor) and  
516 ImageJ<sup>71</sup>.

#### 517 **Secondary structure alignments by amino acids and protein 3D structures**

518 Secondary structures of SrpR and ECF20 were predicted using the JPred4 Server<sup>43</sup>, or modelled via SWISS-  
519 MODEL<sup>72</sup>. SrpR and TetR amino acid sequences were aligned with the known TetR structure (PDB: 4AC0)  
520 using PROMALS3D<sup>45</sup> with default parameters. 3D structures were rendered using the software PyMOL  
521 v1.7.6.7 (Schrodinger).

#### 522 **Library preparation, Next Generation Sequencing and data analysis**

523 Glycerol stocks of the final library were thawed and for each library, 200 µL of the stock was inoculated into  
524 50 mL of fresh medium for overnight growth. Subsequently the plasmid DNA libraries were extracted by  
525 midiprep. For IBM libraries of mCherry, TetR, SrpR and ECF20, appropriate combinations of restriction  
526 enzymes were used to release a minimal length of DNA fragments that contain mixed insertions at various  
527 positions. Digested DNA were resolved on agarose gels and the fragments with mixed insertions, which  
528 migrated as a single band, was excised and purified. For the domain-insertion library of ER-LBD into the  
529 M86 intein which was within mCherry, the region with insertions were amplified by PCR, then resolved and  
530 purified from agarose gels. Purified DNA were sent to Novogene (UK) for fragmentation and sequencing to  
531 obtain at least 7 million reads of 150 bp paired-end per library.

532 The resulting data was processed by in-house developed Python scripts. 12 bp, each at the 5' and 3' termini  
533 of the final inserted DNA were defined as signature sequences. Raw FASTQ files were filtered for reads that  
534 contained perfect matches to these signature sequences. Then, for each filtered read, the signature  
535 sequences were aligned and the adjacent sequence (12 bp) was extracted from the read, which were then  
536 aligned back to the CDS of the target protein to determine insertion positions. Only unique and perfect  
537 matches were considered authentic and a split/insertion site was called. Any fragments where the forward  
538 and reverse reads reported different split/insertion sites were removed, and fragments where the forward  
539 and reverse reads pointed to the same split/insertion site were deduplicated to avoid double counting.  
540 Rare instances of sites mapped beyond the permitted transposition window were also removed. Similar to  
541 previous works, a productive split or insertion site on the amino acid sequence was called only if the  
542 insertion orientation was forward and the insert was in-frame.

#### 543 **Data Processing and Statistics**

544 All data were processed and graphed in Python. Whenever displayed, fluorescence distributions shown  
545 within the same subpanel were normalized to their individual modes. We used two-tailed *t*-tests for  
546 independent samples assuming unequal variances in comparisons of fold changes between median  
547 fluorescent values, and in comparisons of median fluorescent values from populations. Calculation was  
548 done in Python using the SciPy package v1.4.1<sup>73</sup>. Owing to the large number of statistical tests performed  
549 within a single figure panel, we did not report the individual statistics and *P*-values but rather the summary  
550 statistics: n.s., not significant; \*,  $P \leq 0.05$ ; \*\*,  $P \leq 0.01$ ; \*\*\*,  $P \leq 0.001$ . Exact sample sizes (*n*) were described  
551 in figure legends, except for **Supplementary Fig. 17** where sample sizes ( $n \geq 3$ ) of different sites differed  
552 greatly between groups and were too numerous to report as exact values.

#### 553 **Data availability**

554 Source data, including uncropped Western blot images and Python scripts for generating figures, are  
555 deposited to the Edinburgh DataShare (<https://doi.org/10.7488/ds/2954>). Raw sequencing data of IBM and  
556 DIM final libraries from NGS are deposited to the Sequence Read Archive under the project accession code  
557 PRJNA678813. List of constructs used in this study are detailed in Supplementary Data 1, and their  
558 sequences are available on SynBioHub<sup>74</sup>  
559 ([https://synbiohub.org/public/Intein\\_assisted\\_Bisection\\_Mapping/Intein\\_assisted\\_Bisection\\_Mapping\\_coll](https://synbiohub.org/public/Intein_assisted_Bisection_Mapping/Intein_assisted_Bisection_Mapping_collection/1)  
560 [ection/1](https://synbiohub.org/public/Intein_assisted_Bisection_Mapping/Intein_assisted_Bisection_Mapping_collection/1)). Representative key constructs used in this study, which allow researchers to conduct IBM of their  
561 own, are deposited at Addgene (ID 161937-161955). A detailed protocol for carrying out IBM is available at  
562 protocols.io (<https://dx.doi.org/10.17504/protocols.io.bpqdmms6>).

#### 563 **Code availability**

564 Python scripts for analyzing Sanger sequencing results to determine split sites at the final step of IBM, and  
565 for analyzing split or insertion site coverages from NGS data, is available at GitHub  
566 (<https://github.com/tyhho/IBM>).

#### 567 **Acknowledgements**

568 We thank Dr Martin Waterfall from the Flow Cytometry Core Facility at the University of Edinburgh for  
569 performing cells sorting, Dr Hung-Ju Chang and Dr Jerome Bonnet for advice on acVHH-related  
570 experiments, Prof. Bryan C Dickinson for providing plasmids encoding the evolved split T7 RNA polymerase,  
571 members of the Wang and Menolascina labs for helpful discussions, and Dr. Jamie Gilman and Dr. James  
572 Bryson for feedback on the manuscript. We would also like to thank the SBS BioRDM Team for their help  
573 with data deposits and data curation. This work was supported by the UK Research and Innovation Future  
574 Leaders Fellowship [MR/S018875/1], Leverhulme Trust grant [RPG-2020-241] and UK Biotechnology and  
575 Biological Sciences Research Council grant [BB/N007212/1] to B.W.. T.Y.H.H. was supported by the Darwin

576 Trust of Edinburgh and the Edinburgh Global Research Scholarship. A.S. was supported by a Microsoft  
577 Research PhD Scholarship.

## 578 **Author Contributions**

579 B.W. and T.Y.H.H conceived the study. T.Y.H.H developed the methods and designed the experiments with  
580 inputs from B.W., T.Y.H.H, A.S., and Z.L. performed the experiments. T.Y.H.H. analyzed the data with inputs  
581 from B.W., N.D., L.W. and F.M.. H.S. provided the reagents for transposition. All authors took part in the  
582 interpretation of results and preparation of materials for the manuscript. T.Y.H.H. and B.W. wrote the  
583 manuscript with comments from all authors. B.W. supervised and acquired the funding of the study.

## 584 **Competing Interests**

585 The authors declare no competing interests.

586

## 587 **References**

- 588 1. Shekhawat, S.S. & Ghosh, I. Split-protein systems: beyond binary protein–protein interactions. *Current*  
589 *Opinion in Chemical Biology* **15**, 789-797 (2011).
- 590 2. Kamiyama, D. et al. Versatile protein tagging in cells with split fluorescent protein. *Nature*  
591 *Communications* **7**, 11046 (2016).
- 592 3. Guo, Z. et al. Engineered PQQ-Glucose Dehydrogenase as a Universal Biosensor Platform. *Journal of*  
593 *the American Chemical Society* **138**, 10108-10111 (2016).
- 594 4. Hicks, M., Bachmann, T.T. & Wang, B. Synthetic Biology Enables Programmable Cell-Based Biosensors.  
595 *ChemPhysChem* **21**, 132-144 (2020).
- 596 5. Gray, D.C., Mahrus, S. & Wells, J.A. Activation of Specific Apoptotic Caspases with an Engineered Small-  
597 Molecule-Activated Protease. *Cell* **142**, 637-646 (2010).
- 598 6. Weinberg, B.H. et al. High-performance chemical- and light-inducible recombinases in mammalian cells  
599 and mice. *Nature Communications* **10**, 4845 (2019).
- 600 7. Gao, X.J., Chong, L.S., Kim, M.S. & Elowitz, M.B. Programmable protein circuits in living cells. *Science*  
601 **361**, 1252-1258 (2018).
- 602 8. Fink, T. et al. Design of fast proteolysis-based signaling and logic circuits in mammalian cells. *Nature*  
603 *Chemical Biology* **15**, 115-122 (2019).
- 604 9. Xiang, Y., Dalchau, N. & Wang, B. Scaling up genetic circuit design for cellular computing: advances and  
605 prospects. *Natural Computing* **17**, 833-853 (2018).
- 606 10. Wang, B., Kitney, R.I., Joly, N. & Buck, M. Engineering modular and orthogonal genetic logic gates for  
607 robust digital-like synthetic biology. *Nature Communications* **2**, 508 (2011).
- 608 11. Schopp, I.M. et al. Split-BioID a conditional proteomics approach to monitor the composition of  
609 spatiotemporally defined protein complexes. *Nature Communications* **8**, 15690 (2017).
- 610 12. Golob-Urbanc, A., Rajčević, U., Strmšek, Ž. & Jerala, R. Design of split superantigen fusion proteins for  
611 cancer immunotherapy. *Journal of Biological Chemistry* **294**, 6294-6305 (2019).
- 612 13. Ma, D., Peng, S. & Xie, Z. Integration and exchange of split dCas9 domains for transcriptional controls  
613 in mammalian cells. *Nature Communications* **7**, 13056 (2016).
- 614 14. Shah, N.H. & Muir, T.W. Inteins: nature's gift to protein chemists. *Chemical Science* **5**, 446-461 (2014).
- 615 15. Elleuche, S. & Pöggeler, S. Inteins, valuable genetic elements in molecular biology and biotechnology.  
616 *Applied Microbiology and Biotechnology* **87**, 479-489 (2010).

- 617 16. Pinto, F., Thornton, E.L. & Wang, B. An expanded library of orthogonal split inteins enables modular  
618 multi-peptide assemblies. *Nature Communications* **11**, 1529 (2020).
- 619 17. Slomovic, S. & Collins, J.J. DNA sense-and-respond protein modules for mammalian cells. *Nature*  
620 *Methods* **12**, 1085-1090 (2015).
- 621 18. Schaeferli, Y., Gili, M. & Isalan, M. A split intein T7 RNA polymerase for transcriptional AND-logic. *Nucleic*  
622 *Acids Research* **42**, 12322-12328 (2014).
- 623 19. Bradley, R.W., Buck, M. & Wang, B. Tools and Principles for Microbial Gene Circuit Engineering. *Journal*  
624 *of Molecular Biology* **428**, 862-888 (2016).
- 625 20. Wang, T., Badran, A.H., Huang, T.P. & Liu, D.R. Continuous directed evolution of proteins with  
626 improved soluble expression. *Nature Chemical Biology* **14**, 972-980 (2018).
- 627 21. Amitai, G., Callahan, B.P., Stanger, M.J., Belfort, G. & Belfort, M. Modulation of intein activity by its  
628 neighboring extein substrates. *Proceedings of the National Academy of Sciences* **106**, 11005-11010  
629 (2009).
- 630 22. Shah, N.H., Eryilmaz, E., Cowburn, D. & Muir, T.W. Extein Residues Play an Intimate Role in the Rate-  
631 Limiting Step of Protein Trans-Splicing. *Journal of the American Chemical Society* **135**, 5839-5847  
632 (2013).
- 633 23. Davis, K.M., Pattanayak, V., Thompson, D.B., Zuris, J.A. & Liu, D.R. Small molecule-triggered Cas9  
634 protein with improved genome-editing specificity. *Nature Chemical Biology* **11**, 316 (2015).
- 635 24. Jillette, N., Du, M., Zhu, J.J., Cardoz, P. & Cheng, A.W. Split selectable markers. *Nature Communications*  
636 **10**, 4968 (2019).
- 637 25. Palanisamy, N. et al. Split intein-mediated selection of cells containing two plasmids using a single  
638 antibiotic. *Nature Communications* **10**, 4967 (2019).
- 639 26. Dagliyan, O. et al. Computational design of chemogenetic and optogenetic split proteins. *Nature*  
640 *Communications* **9**, 4042 (2018).
- 641 27. Segall-Shapiro, T.H., Meyer, A.J., Ellington, A.D., Sontag, E.D. & Voigt, C.A. A 'resource allocator' for  
642 transcription based on a highly fragmented T7 RNA polymerase. *Molecular Systems Biology* **10**, 742  
643 (2014).
- 644 28. Nadler, D.C., Morgan, S.-A., Flamholz, A., Kortright, K.E. & Savage, D.F. Rapid construction of  
645 metabolite biosensors using domain-insertion profiling. *Nature Communications* **7**, 12266 (2016).
- 646 29. Oakes, B.L. et al. Profiling of engineering hotspots identifies an allosteric CRISPR-Cas9 switch. *Nature*  
647 *Biotechnology* **34**, 646 (2016).
- 648 30. Zeng, Y. et al. A Split Transcriptional Repressor That Links Protein Solubility to an Orthogonal Genetic  
649 Circuit. *ACS Synthetic Biology* **7**, 2126-2138 (2018).
- 650 31. Calles, B. & Lorenzo, V.d. Expanding the Boolean Logic of the Prokaryotic Transcription Factor XylR by  
651 Functionalization of Permissive Sites with a Protease-Target Sequence. *ACS Synthetic Biology* **2**, 594-  
652 603 (2013).
- 653 32. Appleby-Tagoe, J.H. et al. Highly Efficient and More General cis- and trans-Splicing Inteins through  
654 Sequential Directed Evolution. *Journal of Biological Chemistry* **286**, 34440-34447 (2011).
- 655 33. Fan, J.-Y. et al. Split mCherry as a new red bimolecular fluorescence complementation system for  
656 visualizing protein-protein interactions in living cells. *Biochemical and Biophysical Research*  
657 *Communications* **367**, 47-53 (2008).
- 658 34. Thompson, K.E., Bashor, C.J., Lim, W.A. & Keating, A.E. SYNZIP Protein Interaction Toolbox: in Vitro and  
659 in Vivo Specifications of Heterospecific Coiled-Coil Interaction Domains. *ACS Synthetic Biology* **1**, 118-  
660 129 (2012).

- 661 35. Carvajal-Vallejos, P., Pallissé, R., Mootz, H.D. & Schmidt, S.R. Unprecedented Rates and Efficiencies  
662 Revealed for New Natural Split Inteins from Metagenomic Sources. *Journal of Biological Chemistry* **287**,  
663 28686-28696 (2012).
- 664 36. Galarneau, A., Primeau, M., Trudeau, L.-E. & Michnick, S.W.  $\beta$ -Lactamase protein fragment  
665 complementation assays as in vivo and in vitro sensors of protein–protein interactions. *Nature*  
666 *Biotechnology* **20**, 619-622 (2002).
- 667 37. Wehrman, T., Kleaveland, B., Her, J.-H., Balint, R.F. & Blau, H.M. Protein–protein interactions  
668 monitored in mammalian cells via complementation of  $\beta$ -lactamase enzyme fragments. *Proceedings of*  
669 *the National Academy of Sciences* **99**, 3469-3474 (2002).
- 670 38. Beyer, H.M., Mikula, K.M., Li, M., Wlodawer, A. & Iwaï, H. The crystal structure of the naturally split  
671 gp41-1 intein guides the engineering of orthogonal split inteins from cis-splicing inteins. *The FEBS*  
672 *Journal* **287**, 1886-1898 (2020).
- 673 39. Wang, B., Barahona, M. & Buck, M. A modular cell-based biosensor using engineered genetic logic  
674 circuits to detect and integrate multiple environmental signals. *Biosensors and Bioelectronics* **40**, 368-  
675 376 (2013).
- 676 40. Wang, B. & Buck, M. Rapid engineering of versatile molecular logic gates using heterologous genetic  
677 transcriptional modules. *Chemical Communications* **50**, 11642-11644 (2014).
- 678 41. Stanton, B.C. et al. Genomic mining of prokaryotic repressors for orthogonal logic gates. *Nature*  
679 *Chemical Biology* **10**, 99-105 (2014).
- 680 42. Rhodius, V.A. et al. Design of orthogonal genetic switches based on a crosstalk map of  $\sigma$ s, anti- $\sigma$ s, and  
681 promoters. *Molecular Systems Biology* **9**, 702 (2013).
- 682 43. Drozdetskiy, A., Cole, C., Procter, J. & Barton, G.J. JPred4: a protein secondary structure prediction  
683 server. *Nucleic Acids Research* **43**, W389-W394 (2015).
- 684 44. Aranko, A.S., Wlodawer, A. & Iwaï, H. Nature's recipe for splitting inteins. *Protein Engineering, Design*  
685 *and Selection* **27**, 263-271 (2014).
- 686 45. Pei, J., Kim, B.-H. & Grishin, N.V. PROMALS3D: a tool for multiple protein sequence and structure  
687 alignments. *Nucleic Acids Research* **36**, 2295-2300 (2008).
- 688 46. Mootz, H.D. & Muir, T.W. Protein Splicing Triggered by a Small Molecule. *Journal of the American*  
689 *Chemical Society* **124**, 9044-9045 (2002).
- 690 47. Mootz, H.D., Blum, E.S., Tyszkiewicz, A.B. & Muir, T.W. Conditional Protein Splicing: A New Tool to  
691 Control Protein Structure and Function in Vitro and in Vivo. *Journal of the American Chemical Society*  
692 **125**, 10561-10569 (2003).
- 693 48. Di Ventura, B. & Mootz, H.D. Switchable inteins for conditional protein splicing. *Biological Chemistry*  
694 **400**, 467-475 (2019).
- 695 49. Peck, Sun H., Chen, I. & Liu, David R. Directed Evolution of a Small-Molecule-Triggered Inteins with  
696 Improved Splicing Properties in Mammalian Cells. *Chemistry & Biology* **18**, 619-630 (2011).
- 697 50. Skretas, G. & Wood, D.W. Regulation of protein activity with small-molecule-controlled inteins. *Protein*  
698 *Science* **14**, 523-532 (2005).
- 699 51. Gramespacher, J.A., Burton, A.J., Guerra, L.F. & Muir, T.W. Proximity Induced Splicing Utilizing Caged  
700 Split Inteins. *Journal of the American Chemical Society* **141**, 13708-13712 (2019).
- 701 52. Bojar, D., Scheller, L., Hamri, G.C.-E., Xie, M. & Fussenegger, M. Caffeine-inducible gene switches  
702 controlling experimental diabetes. *Nature Communications* **9**, 2318 (2018).
- 703 53. Chang, H.-J. et al. A Modular Receptor Platform To Expand the Sensing Repertoire of Bacteria. *ACS*  
704 *Synthetic Biology* **7**, 166-175 (2018).

- 705 54. Pu, J., Zinkus-Boltz, J. & Dickinson, B.C. Evolution of a split RNA polymerase as a versatile biosensor  
706 platform. *Nature Chemical Biology* **13**, 432-438 (2017).
- 707 55. Stevens, A.J. et al. A promiscuous split intein with expanded protein engineering applications.  
708 *Proceedings of the National Academy of Sciences* **114**, 8538-8543 (2017).
- 709 56. Dagliyan, O. et al. Rational design of a ligand-controlled protein conformational switch. *Proceedings of*  
710 *the National Academy of Sciences* **110**, 6800-6804 (2013).
- 711 57. Karginov, A.V., Ding, F., Kota, P., Dokholyan, N.V. & Hahn, K.M. Engineered allosteric activation of  
712 kinases in living cells. *Nature Biotechnology* **28**, 743-747 (2010).
- 713 58. Buskirk, A.R., Ong, Y.-C., Gartner, Z.J. & Liu, D.R. Directed evolution of ligand dependence: Small-  
714 molecule-activated protein splicing. *Proceedings of the National Academy of Sciences of the United*  
715 *States of America* **101**, 10505-10510 (2004).
- 716 59. Brödel, A.K., Jaramillo, A. & Isalan, M. Intracellular directed evolution of proteins from combinatorial  
717 libraries based on conditional phage replication. *Nature Protocols* **12**, 1830-1843 (2017).
- 718 60. Mizuuchi, M. & Mizuuchi, K. Target Site Selection in Transposition of Phage Mu. *Cold Spring Harbor*  
719 *Symposia on Quantitative Biology* **58**, 515-523 (1993).
- 720 61. Haapa-Paananen, S., Rita, H. & Savilahti, H. DNA Transposition of Bacteriophage Mu: A QUANTITATIVE  
721 ANALYSIS OF TARGET SITE SELECTION IN VITRO. *Journal of Biological Chemistry* **277**, 2843-2851 (2002).
- 722 62. Manna, D., Deng, S., Breier, A.M. & Higgins, N.P. Bacteriophage Mu Targets the Trinucleotide Sequence  
723 CGG. *Journal of Bacteriology* **187**, 3586-3588 (2005).
- 724 63. Green, B., Bouchier, C., Fairhead, C., Craig, N.L. & Cormack, B.P. Insertion site preference of Mu, Tn5,  
725 and Tn7 transposons. *Mobile DNA* **3**, 3 (2012).
- 726 64. Coyote-Maestas, W., Nedrud, D., Okorafor, S., He, Y. & Schmidt, D. Targeted insertional mutagenesis  
727 libraries for deep domain insertion profiling. *Nucleic Acids Research* **48**, e11-e11 (2019).
- 728 65. Atkinson, J.T., Jones, A.M., Zhou, Q. & Silberg, J.J. Circular permutation profiling by deep sequencing  
729 libraries created using transposon mutagenesis. *Nucleic Acids Research* **46**, e76-e76 (2018).
- 730 66. Baker, T.A., Mizuuchi, M., Savilahti, H. & Mizuuchi, K. Division of labor among monomers within the  
731 Mu transposase tetramer. *Cell* **74**, 723-733 (1993).
- 732 67. Haapa-Paananen, S. & Savilahti, H. Applications of the Bacteriophage Mu In Vitro Transposition  
733 Reaction and Genome Manipulation via Electroporation of DNA Transposition Complexes. *Methods in*  
734 *Molecular Biology* **1681**, 279-286 (2018).
- 735 68. Engler, C., Kandzia, R. & Marillonnet, S. A One Pot, One Step, Precision Cloning Method with High  
736 Throughput Capability. *PLOS ONE* **3**, e3647 (2008).
- 737 69. Cock, P.J.A. et al. Biopython: freely available Python tools for computational molecular biology and  
738 bioinformatics. *Bioinformatics* **25**, 1422-1423 (2009).
- 739 70. Kunzmann, P. & Hamacher, K. Biotite: a unifying open source computational biology framework in  
740 Python. *BMC Bioinformatics* **19**, 346 (2018).
- 741 71. Rueden, C.T. et al. ImageJ2: ImageJ for the next generation of scientific image data. *BMC*  
742 *Bioinformatics* **18**, 529 (2017).
- 743 72. Bienert, S. et al. The SWISS-MODEL Repository—new features and functionality. *Nucleic Acids Research*  
744 **45**, D313-D319 (2016).
- 745 73. Virtanen, P. et al. SciPy 1.0: fundamental algorithms for scientific computing in Python. *Nature*  
746 *Methods* **17**, 261-272 (2020).
- 747 74. McLaughlin, J.A. et al. SynBioHub: A Standards-Enabled Design Repository for Synthetic Biology. *ACS*  
748 *Synthetic Biology* **7**, 682-688 (2018).